Applied Thermal Engineering 231 (2023) 120944

Contents lists available at ScienceDirect

Applied Thermal Engineering

journal homepage: www.elsevier.com/locate/apthermeng

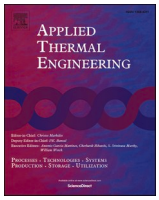

Research Paper

A modified ε-NTU analytical model for the investigation of counter-flow Maisotsenko-based cooling systems

Alberto Muscio *, Michele Cossu, Nicolò Morselli, Marco Puglia, Simone Pedrazzi, Giulio Allesina

BEELab (Bio Energy Efficiency Laboratory), Department of Engineering "Enzo Ferrari", University of Modena and Reggio Emilia, Via Vivarelli 10/1, 41125 Modena, Italy

ARTICLE INFO

Keywords:
Maisotsenko cycle
Indirect evaporative cooling
ε-NTU method
Dew point temperature

ABSTRACT

In this work the *ε-NTU* method has been adapted for the application of a countercurrent evaporative heat exchanger featuring a complex heat transfer surface. The study highlights some challenges related to extending analytical models that were validated on simple geometries and proposes the calibration of the *ε-NTU* method by experimentally measuring the overall heat transfer coefficient (*UA*) of the heat exchanger. Through a laboratory prototype of the M-cycle, two different operating conditions were investigated (mild and hot-dry climates) which reported almost constant *UA* values of 14.8 W/K and 16.1 W/K respectively. The obtained results from the model prediction were compared with the experimental data obtaining average errors on the outlet temperatures and on the cooling capacity lower than 1.5% in the case of simulation of hot and dry climate. The positive results allowed to extend the calculation to operating conditions not tested experimentally, highlighting how it is necessary to have NTU over 2–2.5, while the recirculation rate must be kept below 0.4 to make efficient use of the water. The aim is to support the implementation of the technology in full-scale applications, where the M-cycle is used alone or to complement a vapor compression system.

1. Introduction

Global warming and the continuous increase in violent meteorological effects such as persistent heat waves bring the issue of cooling domestic, industrial and agricultural environments to the fore. The constant improvement of the socio-economic conditions of many countries has resulted in an exponential increase in the diffusion of air conditioning systems. The IEA 2022 report [1] highlights how energy consumption for space cooling has more than tripled since 1990, accounting for around 16% of total electricity consumption for the building sector in 2021 (2 GWh). At the same time, total CO_2 equivalent emissions increased from 566 to 994 $MtCO_2$. This scenario of constant growth in energy consumption and greenhouse gas emissions should be included in the framework of the European Green Deal [2] which aims to a 55% net greenhouse gas emissions reduction by 2030, compared to 1990 levels and the carbon-neutrality by 2050. To achieve this, it is estimated that the emission intensity (average CO_2 emissions per cooling unit) needs to be reduced to about 1/3, driving research towards new cooling systems.

The cooling systems currently used are mostly vapor compression refrigeration systems (VCRs), which use refrigerants (*i.e.* R134A, R22, etc.) to remove heat from the refrigerated environment. In this architecture, the latent heat of condensation/vaporization associated with the phase change of the refrigerant allow heat extracion from a low-temperature environment (the space requiring cooling) and transfer it to a higher-temperature environment (typically the external environment).

Due to the necessary compression of the refrigerant fluid, this process is characterized by a high electrical energy consumption, leading to the VCR architecture to be considered not an ecological and sustainable technology [3]. Despite the evolution of these systems over the years, the coefficient of performance (COP) is on average between 2 and 5 [4] and the use of refrigerant fluids remains one of the primary reasons for the increase in the planet's greenhouse effect [5].

The low-energy alternative for space cooling can be found in evaporative systems, which use the latent heat of vaporization of water to reduce the temperature of (typically) an air flow. These systems can be divided into two macro-groups according to the psychrometric cycle architecture: direct evaporative cycles (DEC) and indirect evaporative

* Corresponding author.
E-mail address: alberto.muscio@unimore.it (A. Muscio).

https://doi.org/10.1016/j.applthermaleng.2023.120944
Received 11 January 2023; Received in revised form 12 April 2023; Accepted 8 June 2023
Available online 13 June 2023

Nomenclature

A	heat transfer area (m^2)
C	heat capacity (J/K)
C_r	heat capacity ratio (–)
c_p	specific heat at constant pressure (J/(kg·K))
$c_{p,eq}$	equivalent specific heat at constant pressure (J/(kg·K))
c_w	liquid water specific heat (J/(kg·K))
J	moist air specific enthalpy (J/kg)
$\dot{m}$	mass flow rate (kg/s)
NTU	number of heat transfer units (–)
p	pressure (Pa)
Q	heat transfer rate (W)
Q_{max}	maximum heat transfer rate (W)
q_{lv}	latent heat of vaporization/condensation of water (J/kg)
R	gas constant (J/(kg·K))
r	recirculation ratio (–)
T	Temperature (K)
T_w	liquid water temperature (K)
U	overall heat transfer coefficient (W/(m^2·K))
V	volume flow rate (m^3/s)
x	absolute humidity (kg_v/kg_a)

Greek symbols

ε	effectiveness (–)
ρ	density (kg/m^3)
φ	relative humidity (–)

Subscripts

amb	ambient
a	air
v	water vapour
dry	dry duct
wet	wet duct
in	inlet section
out	outlet section
sat	saturation
wb	wet bulb
dp	dew point

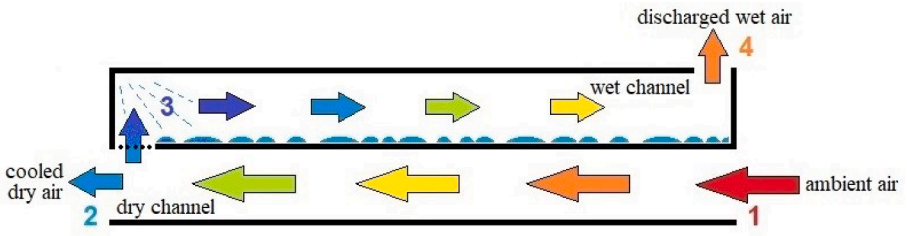

Fig. 1. Key-points of the Maisotsenko cycle: 1) suctioned ambient air; 2) cooled non-humidified air; 3) cooled humidified air; 4) discharged moist air.

cycles (IEC).

In DEC, the air flow to be cooled comes into direct contact with the water to be evaporated, ideally reaching saturation conditions. The main disadvantage of this design is the increase in water content of the air flow, leading to a rise in humidity levels in the environmental space being cooled. This can cause discomfort and dangerous mold formations on the walls [6] and may even lead to health problems due to suspended contaminated water droplets that can favor the growth of pathogens (e.g. *Legionella*) [7,8]. Although the theoretical minimum temperature achievable for the outlet air is the wet bulb temperature of the treated air, the literature suggests that a wet bulb effectiveness ranging between 70 and 95% is more feasible [9].

In IEC, the air intended for room cooling is cooled in a heat and mass exchanger (HMX) through a separate and humidified air stream. The advantage of IEC over DEC is that it avoids the strong humidification of the air introduced into the building. However, the effectiveness of the IEC is further decreased when compared to the DEC due to the thermal resistances introduced by the HMX, with values between 40 and 60% [9].

Among IEC cycles, the Maisotsenko's cycle (M-cycle) which takes its name from the inventor who designed it in 1976 (Patent # SU979796) [10] is considered highly innovative due to its ability to achieve high efficiency and low energy consumption. The M-cycle is a dew point evaporative cooling (DPEC) in which part of the indirectly cooled air is recirculated in the wet channel of the HMX, increasing the overall effectiveness of heat exchange. Thanks to this strategy, it is possible to obtain wet bulb effectiveness higher than 100% setting the dew point temperature as the temperature limit (Fig. 1).

Over the years, several experimental [9,11,12,13] and numerical [6,14,15,16,17,18,19] studies have been performed and many architectures have been conceived, including regenerative counter-current [12,14], counter-current with complete separation between working air and product air [15], counter-current with perforations along the entire channel [18] and cross-flow with different perforation arrangements [3,6,13]. On average, the validations of the numerical models available in the literature have an accuracy of around 10%.

Riangvilaikul & Kumal [9] realized an experimental apparatus with counter-current flows, 1200 mm long, oriented vertically so that water flows into the wet channel from above by gravity, recovering the excess water on the bottom. Subsequently, they developed a numerical model [14] to predict the behavior of the M-cycle as the air inlet conditions varied. Between experimental and theoretical data, they observed a discrepancy of less than 5% for the outlet temperatures of the product air and less than 10% for wet bulb effectiveness. The results obtained from the authors' experiments were then used several times to compare the different mathematical models [16,19,20].

Bakeem et al. developed a 1D numerical model and investigated the performance of a counterflow HMX in the climates of some important cities of the Arabian Peninsula throughout the year [16]. They observed that in all the studied cases it was possible to exceed 100% for the wet bulb effectiveness. They then investigated the effects of different duct geometries [17] concluding that the best results could be obtained with triangular and cylindrical cross sections.

Cui et al. [15] also developed a 1D numerical model for a counter-flow HMX. In their model, the airflow is implemented as a continuous phase with an Eulerian approach and solved with Navier-Stokes equations, while water droplets are implemented as a discrete phase with a Lagrangian approach. The mass exchange is then treated as a source of

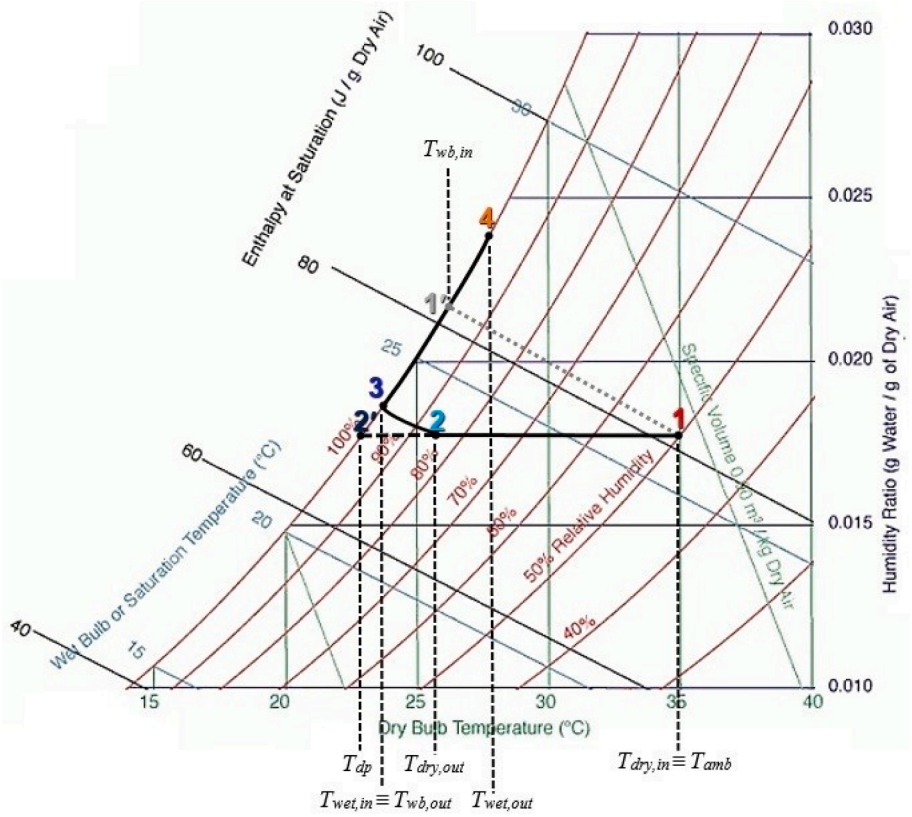

Fig. 2. Psychrometric chart and key-points of the M-cycle: 1) suctioned ambient air; 2) cooled non-humidified air; 3) cooled humidified air; 4) discharged moist air; 1′) wet-bulb temperature at ambient and inlet conditions; 2′) dew point temperature.

mass in the continuous phase continuity equation and as a source of water vapor in the transport equation. The heat transferred by the continuous phase of the airflow is treated as an energy source/sink in the energy balance equation. The model was then validated with the experimental results of Hsu et al. [21] and of Kozubal et al. [22,23] obtaining an error of less than 8% for the outlet temperature compared to the experimental data.

Zhu et al. [18] developed a numerical model for an M-cycle HMX in which the working air has a portion of dry channel and a portion of wet channel connected by perforations along the entire length of the M-cycle and both kept separate from the product air. In their work, a correlation between dew point effectiveness and dimensionless variables that affect the system performance is identified. The correlation is determined through a nonlinear regression based on numerical data obtained through CFD. The discrepancy is less than 9% and 14% when compared to numerical and experimental results respectively, making it a useful way to approach complex systems with adequate precision and time-saving compared to numerical modeling.

Mathematical models that describe the performance of the M-cycle are based on various assumptions, among which the most widespread is that of considering the injected water uniformly distributed on the heat transfer surface. In practical applications this condition is hard to achieve and researchers adopted different methods to satisfy this assumption, for example sheet of polyurethane covered with cotton [9], aluminum sheets coated with fabric [11], felt [13], or other porous layer [12]. On the other hand, numerical analyses were carried out to evaluate the effect of the lack of water on some portions of the exchange surface [19].

The literature analysis reveals that a significant amount of research has focused on the development of numerical models, which typically require high computation times. On the other hand, there have been few attempts to develop analytical models that could serve as a quick and efficient tool for studying evaporative coolers based on M-cycles [5].

To the best of our knowledge, only Hasan (2012) [24] and Liu et al. (2013) [20] have developed a pure analytical model based on ε-NTU methodology. In these models, simplifications are developed for the calculation of NTU to describe the sensible and latent behaviour of the water film that forms and evaporates on the surface of the wet duct. The authors aim is to modify the parameters of the ε-NTU model for sensible heat exchangers to establish a correlation between the temperature in the dry channel and the enthalpy in the wet channel. However, correlations often hold true for heat transfer surfaces with simple and regular geometries: Hasan [24] and Liu et al. [20] used experimental data from tests on rectangular channels with fully developed flows. Nevertheless, the simplifications adopted in such research are often strong and difficult to verify, according to the authors themselves. The Lewis number is often set equal to 1 and the Nusselt number is often considered constant along the entire channel in cases of laminar flow.

The purpose of this work is to develop an analytical method that can be applied in HMX with complex heat transfer surfaces, whose operating conditions deviate from the cases evaluated in the models available in literature. To achieve this, a lab-scale HMX prototype was made to replicate the operating principle of the M-cycle. The HMX is composed of two adjacent channels that are insulated from the outside and separated by a thin aluminum wall coated with biochar powder on the wet side to increase the amount of retained water. Biochar is a highly porous carbonaceous material known for its high water retention capacity [25,26]. The heat transfer surface was made by extruding a corrugated profile to increase the surface area, a construction technique commonly used in DEC.

The experimental value of the overall heat transfer coefficient (UA) was investigated by the test rig under two different conditions: one simulating a mild climate (22 °C and 29% RH) while the other simulating a hot and dry climate (40 °C and 10% RH). The collected data

show that, while maintaining a constant air flow rate to the HMX, UA varies little depending on the inlet air conditions and the working to total air mass flow rate with a maximum of 16.6 W/K and a minimum of 14.3 W/K.

The mixed analytical-experimental approach on the model can also predict the cooling capacity with excellent accuracy, with average errors of 11.5% and 14.3% for high and low temperature tests respectively. The same cannot be said for the current available ε-NTU models, which use subroutines to calculate UA based on unverifiable assumptions about HMX with complex geometries, leading to unacceptable discrepancies when applied to the considered test rig.

The following chapters describe the method and experimental apparatus used for the validation of the proposed analytical approach. Finally, the model was used to extend the results beyond the tested conditions, highlighting that recirculation rates higher than 0.4 are disadvantageous in terms of water utilization efficiency. However, to obtain product air outlet temperatures lower than the wet bulb temperature, it is necessary to reach NTU values higher than 2–2.5.

2. Materials and methods

2.1. Modified ε-NTU analytical model

The mathematical model is based on the simplest counter flow M-cycle architecture described in Fig. 1 and follows the psychrometric transformation represented in Fig. 2, where 1–2 is the cooling phase in the dry channel, 2 or 3 is the release temperature, and 2′ is the dew point temperature. Moreover, 3–4 is the progressive warming and saturation phase in the wet channel. An adiabatic saturation process from the initial ambient conditions (1) to the corresponding wet-bulb temperature (1′) is also shown as a dashed line.

Ambient air is suctioned into the dry channel at temperature $T_{dry,in}$ (°C) and relative humidity $\varphi_{dry,in}$ (%), then it is cooled down and exits the dry channel at temperature $T_{dry,out}$ (°C). The absolute humidity, or humidity ratio, defined as the mass of water vapor in the unit of mass of dry air, does not change along the dry channel, so that its value at the outlet $x_{dry,out}$ (kg_v/kg_a) is equal to the inlet value $x_{dry,in}$ (kg_v/kg_a). The latter is calculated from the inlet (*i.e.* ambient) conditions by the well-known formula:

$$x_{dry,out} \equiv x_{dry,in} = 0.622 \cdot \frac{p_{v,dry,in}}{p_{amb} - p_{v,dry,in}} \tag{1}$$

where p_{amb} (Pa) is the absolute ambient pressure, and the water vapor partial pressure $p_{v,in}$ (Pa) is calculated from $\varphi_{dry,in}$ and the saturation pressure of water $p_{sat,in}$ (Pa):

$$p_{v,dry,in} = \phi_{dry,in} \cdot p_{sat,in} \tag{2}$$

A commonly used empirical equation [27] for calculation of $p_{sat,in}$ is:

$$p_{sat,in} \approx 610.5 \cdot \exp\left(17.269 \cdot \frac{T_{dry,in}}{237.3 + T_{dry,in}}\right) \tag{3}$$

In the M-cycle configuration of Figs. 1-2, a mass fraction r ($0 < r < 1$) of the cooled air is diverted into the wet channel, and the remaining fraction ($1 - r$) is supplied to the environment to be cooled. Since the absolute humidity does not change in the dry channel ($x_{dry,out} \equiv x_{dry,in}$), and so the partial pressure of water vapor does ($p_{v,dry,out} \equiv p_{v,dry,in}$), the relative humidity $\varphi_{dry,out}$ (%) at the dry channel outlet is such that:

$$\varphi_{dry,out} = \frac{p_{v,dry,out}}{p_{sat,out}} \equiv \frac{p_{v,dry,in}}{p_{sat,out}} \tag{4}$$

where the saturation pressure of water $p_{sat,out}$ (Pa) at the outlet temperature $T_{dry,out}$ can be calculated by a formula analogous to that used for $p_{sat,in}$ as given in Eq. (3). $T_{dry,out}$ cannot fall below the dew point temperature T_{dp} (°C) (*i.e.* $T_{dry,out} \geq T_{dp}$). The dew point temperature corresponding to the vapor partial pressure $p_{v,dry,in}$ at the dry channel inlet can be calculated by reversing the correlation in Eq. (3):

$$T_{dp} \approx \frac{237.3}{\frac{17.269}{ln\left(\frac{p_{v,dry,in}}{610.5}\right)} - 1} \tag{5}$$

In this regard, a dew point efficiency $\eta_{dp,dry}$ (%) for the M-cycle in which cooled dry air is released can be defines as follows:

$$\eta_{dp,dry} = 100 \cdot \frac{T_{dry,in} - T_{dry,out}}{T_{dry,in} - T_{dp}} \tag{6}$$

In case the cooled air is saturated before being released, a dew point efficiency $\eta_{dp,wet}$ (%) can also be defined:

$$\eta_{dp,wet} = 100 \cdot \frac{T_{dry,in} - T_{wet,in}}{T_{dry,in} - T_{dp}} \tag{7}$$

The ideal dew point efficiency can be estimated by numerical modelling of the heat exchanger. However, an alternative analytical approach is proposed here. It is based on the reasonable assumption that the fraction of cooled dry air that is diverted in the wet channel undergoes an adiabatic saturation in the very first part of the wet channel (stage 2–3 in Fig. 2), thereafter it is warmed up along the wet channel by heat transfer from the dry channel (stage 3–4). Moreover, liquid water is continuously evaporated along the wet channel and the air is always kept close to saturation, so most of the heat is absorbed as latent heat and the process follows the saturation curve. In the initial adiabatic saturation (2–3), the wetted air can theoretically be cooled down to the wet-bulb temperature $T_{wb,out}$ (°C) corresponding to the dry-bulb temperature and relative humidity of the cooled dry air, $T_{dry,out}$ and $\phi_{dry,out}$. As explained in the following, $T_{wb,out}$ controls $T_{dry,out}$ as it is the same temperature $T_{wet,in}$ (°C) of the air introduced in the wet channel ($T_{wet,in} \equiv T_{wb,out}$) and thus used to cool down in counter flow the air flowing in the dry channel. The advantage of the M-cycle is that either $T_{wb,out}$ or $T_{dry,out}$ are lower than the wet-bulb temperature $T_{wb,in}$ (°C) corresponding to the dry-bulb temperature and relative humidity of the dry air prior to be cooled, that is the minimum temperature allowed by a standard evaporative cooling system, be it direct or indirect.

The specific enthalpy $J_{wet,in}$ (J/kg_a) of the air-vapor mixture after the initial adiabatic saturation, referred to the unit mass of dry air, must equal the specific enthalpy of the air-vapor mixture $J_{dry,out}$ (J/kg_a) immediately before saturation, that is that at the outlet of the dry channel, slightly increased by the sensible heat of the evaporated liquid water:

$$J_{wet,in} = J_{dry,out} + \left(x_{wet,in} - x_{dry,out}\right) \cdot c_w \cdot T_w \approx J_{dry,out} \tag{8}$$

where

$$J_{dry,out} = c_{p,a} \cdot T_{dry,out} + x_{dry,out} \cdot \left(c_{p,v} \cdot T_{dry,out} + q_{lv}\right) \tag{9}$$

Liquid water is sprayed in the airflow and excess liquid is collected and recirculated, therefore, after an initial transient in which the liquid starts being at ambient temperature, this is cooled down to the wet bulb temperature immediately after the initial adiabatic saturation ($T_w \approx T_{wet,in}$). However, in Eq. (8) it is shown that, with a generally accepted approximation, the sensible heat of the evaporated liquid water can be neglected in view of the small temperature change. The initial saturation may not be exactly adiabatic as some heat may come from the dry channel. Nonetheless, for sake of simplicity, this heat can be assumed to be transferred after that the initial saturation has been completed, abiding the energy conservation.

The specific enthalpy J_{sat} of the air-vapor mixture along the saturation curve is related to the temperature T (°C) and, through the saturation pressure of water p_{sat} (Pa), to the saturation absolute humidity x_{sat} (kg_v/kg_a):

$$J_{sat}(T) = c_{p,a} \cdot T_{dry,out} + x_{sat}(T) \cdot \left(c_{p,v} \cdot T + q_{lv}\right)$$

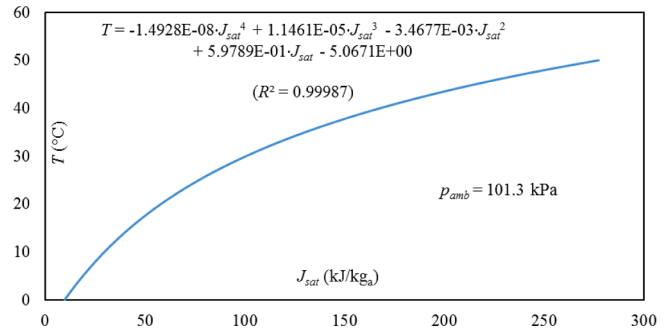

Fig. 3. Correlation between temperature and specific enthalpy J_{sat} of the saturated air-vapor mixture (sea level ambient pressure).

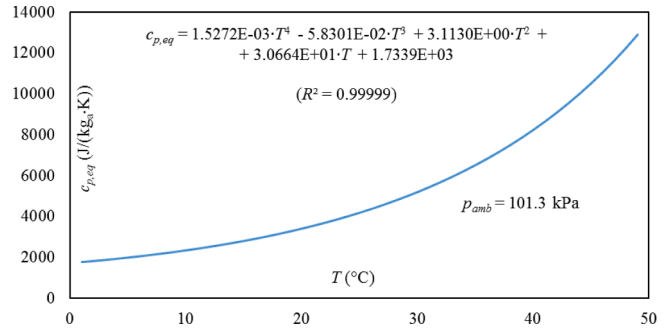

Fig. 4. Correlation between equivalent specific heat at constant pressure $c_{p,eq}$ of the saturated air and temperature (sea level ambient pressure).

$$x_{sat} = 0.622 \cdot \frac{p_{sat}(T)}{p_{amb} - p_{sat}(T)}$$
$$p_{sat}(T) = 610.5 \cdot \exp\left(17.269 \cdot \frac{T}{237.3 + T}\right) \quad (10)$$

The correlation between J_{sat} (J/kg$_a$) and T (°C) on the saturation curve ($\phi = 100\%$) is one-to-one. It can be calculated at the given ambient pressure p_{amb} and thereafter expressed by the polynomial reported in Fig. 3 and Eq. (11), automatically recalculated by the model according to the ambient pressure measured or estimated.

$$T = -1.4928E-08 \cdot J_{sat}^4 + 1.1461E-05 \cdot J_{sat}^3 - 3.4677E-03 \cdot J_{sat}^2 + +5.9789E-01 \cdot J_{sat} - 5.0671E+00 \quad (11)$$

An equivalent specific heat at constant pressure $c_{p,eq}$ (J/(kg$_a$·K)), including sensible and latent heat and referred to the mass unit of dry air, is also associated to the temperature increase of the air-vapor mixture along the saturation curve.

$$c_{p,eq}(T) = \frac{dJ_{sat}(T)}{dT} \quad (12)$$

Due to latent heat effects, $c_{p,eq}$ is much larger than the specific heat at constant pressure of dry air $c_{p,a}$, moreover it is highly temperature dependent. The correlation with temperature (at the given ambient pressure p_{amb}) can again be expressed by the polynomial reported in Fig. 4 and Eq. (13).

$$c_{p,eq} = 1.5272E-03 \cdot T^4 - 5.8301E-02 \cdot T^3 + 3.1130E+00 \cdot T^2 + 3.0664E+01 \cdot T + 1.7339E+03 \quad (13)$$

Heat is transferred between dry flow and wet flow in the counter flow heat exchanger. This is analyzed by means of the ε-*NTU* method. In this regard, an instantaneous heat capacity C_{dry} (W/K) of the dry air flow is:

$$C_{dry} = \dot{m}_a \cdot (c_{p,a} + x_{dry} \cdot c_{p,v}) \quad (14)$$

The mass flow rate of cooled dry air can be calculated from the volume flow rate $\dot{V}_{in}$ (m^3/s) of the ambient air and the dry air density ρ_a (kg$_a$/m^3) at the inlet of the dry channel:

$$\dot{m}_a = \rho_a \cdot \dot{V}_{in} \quad (15)$$

where

$$\rho_a = \frac{p_{amb} - \varphi_{dry,in} \cdot p_{sat,in}}{R_a \cdot T_{dry,in}} \quad (16)$$

and R_a (J/(kg$_a$·K)) is the perfect gas constant of the dry air.

An instantaneous heat capacity C_{wet} (W/K) of the wet air flow can also be defined:

$$C_{wet} = r \cdot \dot{m}_a \cdot c_{p,eq,mean} \quad (17)$$

Since the equivalent specific heat $c_{p,eq}$ changes significantly with temperature (see Fig. 4), a mean value $c_{p,eq,mean}$ (J/(kg$_a$·K)) has been introduced in the relationship above. This is unknown in principle as the outlet conditions of the wet channel are also unknown. An initial estimate that was found effective consists of calculating the value of $c_{p,eq}$ at the wet bulb temperature of the ambient air $T_{wb,in}$ (°C). Such temperature is mostly intermediate between the temperature $T_{wet,in}$ after dry cooling and initial saturation and the temperature $T_{wet,out}$ of the wet air flow before it is discharged from the HMX. The estimate can then be refined from the calculated outlet conditions of the wet channel, possibly through an iterative approach:

$$c_{p,eq,mean} \approx \frac{J_{wet,out} - J_{wet,in}}{T_{wet,out} - T_{wet,in}} \quad (18)$$

In the ε-*NTU* method, the effectiveness ε (%) of the heat exchange process is defined as the ratio of the achieved heat transfer rate and the maximum theoretical one, for which the fluid with the lowest instantaneous heat capacity exits at the inlet temperature of the other fluid. With reference to the M-cycle, one has:

$$\varepsilon = \frac{\dot{Q}}{\dot{Q}_{max}} = \frac{\dot{Q}}{C_{min} \cdot (T_{dry,in} - T_{wet,in})} \quad (19)$$

The ε-*NTU* method requires that a minimum instantaneous heat capacity is identified, for which that of the dry flow seems a convenient choice as it does not change during the dry cooling stage (1–2). Instead, the instantaneous heat capacity of the wet flow depends on $c_{p,eq,mean}$. Since this is much higher than that of the air (Fig. 4), the instantaneous heat capacity of the wet flow is higher than that of the dry flow even if the fraction r of the air flow that is diverted from the dry channel into the wet channel is relatively low. In particular, a minimum value of r exists, for which C_{dry} does not exceeds C_{wet}:

$$C_{dry} \le C_{wet} \leftrightarrow \dot{m}_a \cdot (c_{p,a} + x_{dry,in} \cdot c_{p,v}) \le r \cdot \dot{m}_a \cdot c_{p,eq,mean} \rightarrow r \ge \frac{c_{p,a} + x_{dry,in} \cdot c_{p,v}}{c_{p,eq,mean}} \quad (20)$$

The above condition is generally satisfied in the M-cycle systems, where $r > 0.4$. As a result, the effectiveness ε of the counter-flow heat exchanger depends on the ratio of the instantaneous heat capacities and the number of transfer units *NTU* as follows:

$$\varepsilon\left(\frac{C_{min}}{C_{max}}, NTU\right) = \frac{1 - \exp\left[-NTU \cdot \left(1 - \frac{C_{dry}}{C_{wet}}\right)\right]}{1 - \left(\frac{C_{dry}}{C_{wet}}\right) \cdot \exp\left[-NTU \cdot \left(1 - \frac{C_{dry}}{C_{wet}}\right)\right]} \quad (21)$$

The number of transfer units *NTU* is defined as:

$$NTU = \frac{U \cdot A}{C_{min}} \quad (22)$$

where U (W/(m^{2}K)) is the overall heat transfer coefficient between the two channels, through the separating wall, and A (m^2) is the effective heat transfer area of the separating wall.

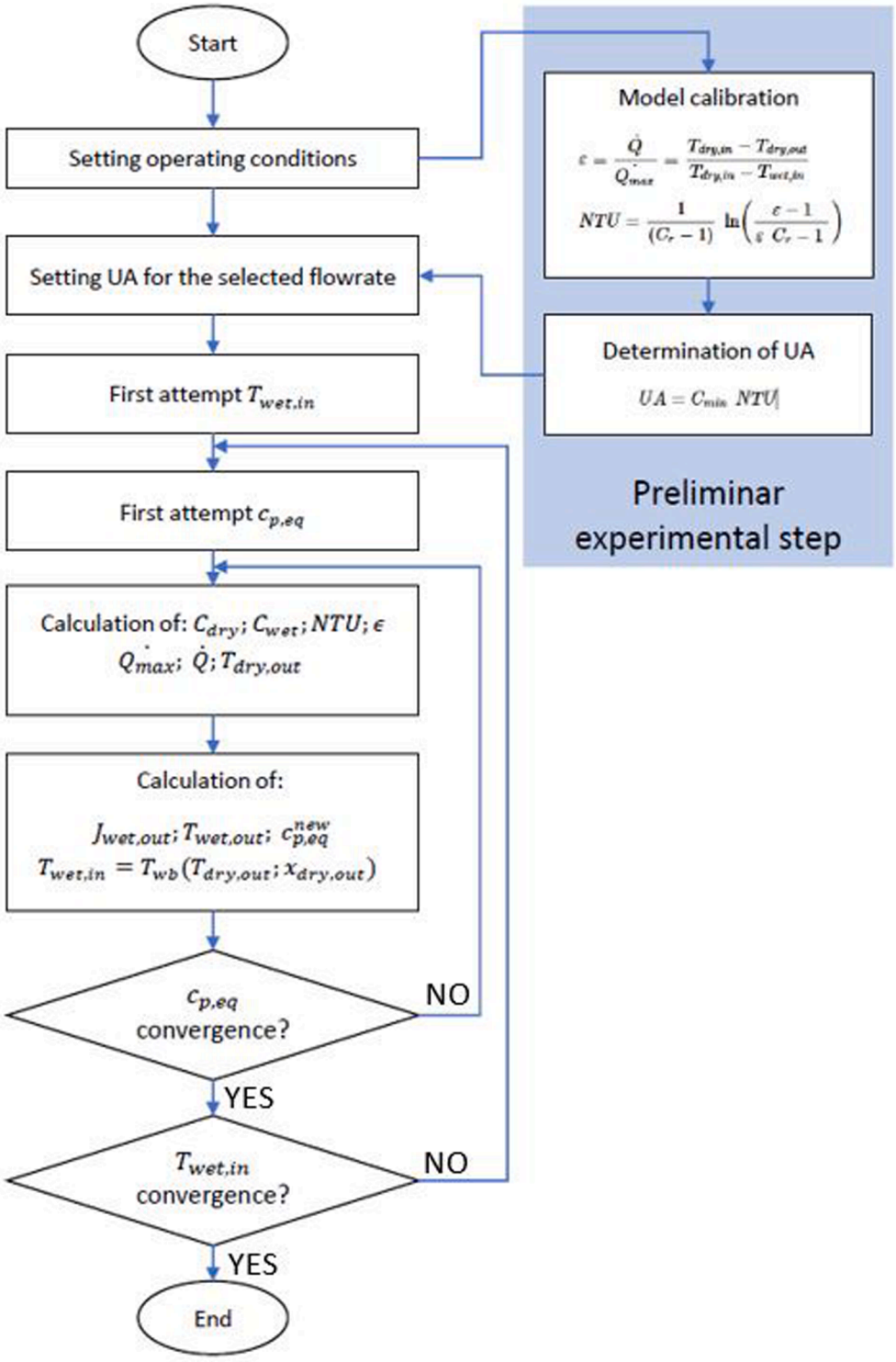

Fig. 5. Flowchart of the experimental-analytical process.

In the M-cycle, the maximum heat transfer rate that could be exchanged between the two air flows is that at which the dry air enters the dry channel at inlet/ambient temperature $T_{dry,in} \equiv T_{amb}$ and exits at the wet bulb temperature $T_{wet,in} \equiv T_{wb,out}$ after an adiabatic saturation of the cooled dry air. The latter is the temperature at which a fraction r of the mass flow rate enters the wet channel, while the remaining air is supplied to the cooled environment. As the heat rate that is actually exchanged is that at which the dry air exits at temperature $T_{dry,out}$, one has for $C_{min} \equiv C_{dry}$:

$$\varepsilon = \frac{\dot{Q}}{\dot{Q}_{max}} = \frac{C_{dry} \cdot (T_{dry,in} - T_{dry,out})}{C_{min} \cdot (T_{dry,in} - T_{wet,in})} \equiv \frac{T_{dry,in} - T_{dry,out}}{T_{dry,in} - T_{wet,in}} \tag{23}$$

With ambient conditions assigned in terms of $T_{dry,in} \equiv T_{amb}$, $\phi_{dry,in} \equiv \phi_{amb}$, and p_{amb}, from which $x_{dry,in} = x_{dry,out}$ and $p_{v,dry,in} = p_{v,dry,out}$, a one-to-one correlation exists between $T_{dry,out}$ and $T_{wet,in}$. As a results, a unique couple of $T_{dry,out}$ and $T_{wet,in}$ values exists for a given value of ε. With assigned ambient conditions, a unique value also exists for the dew

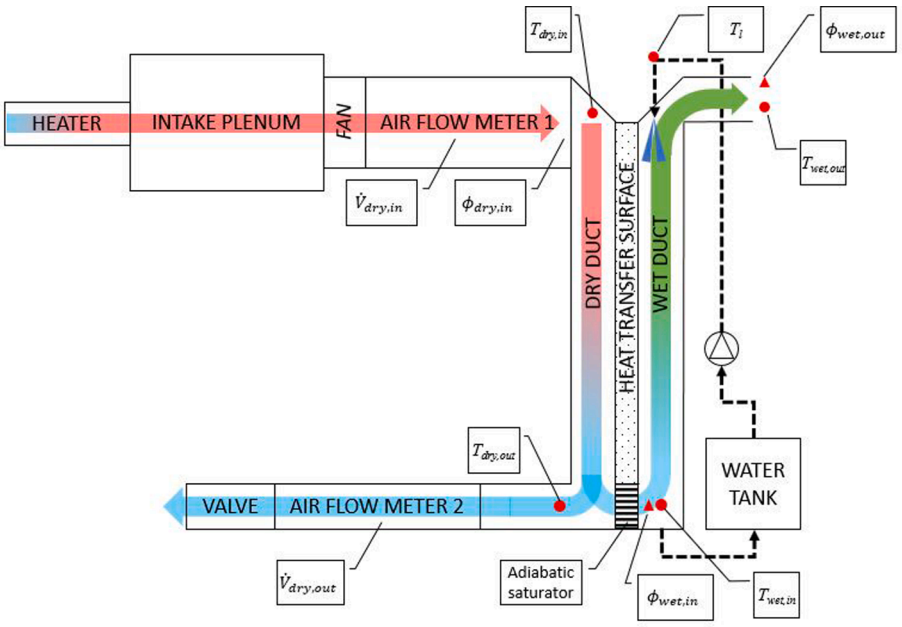

Fig. 6. Schematic representation of the test rig.

point temperature T_{dp}, and, consequently, for dew point effectiveness as expressed in eq. (7)–(8).

Finally, the enthalpy $J_{wet,out}$ (J/kg$_a$) of the air-vapor mixture at the wet channel outlet can be calculated in order to improve the estimate of $c_{p,eq,mean}$:

$$\dot{Q} = C_{dry}\cdot\left(T_{dry,in} - T_{dry,out}\right) \equiv \dot{m}_a\cdot\left(c_{p,a} + x_{dry,in}\cdot c_{p,v}\right)\cdot\left(T_{dry,in} - T_{dry,out}\right) = r\cdot\dot{m}_a\cdot\left(J_{wet,out} - J_{wet,in}\right) \quad (24)$$

from which:

$$J_{wet,out} = J_{wet,in} + \frac{\dot{Q}}{r\cdot\dot{m}_a} = J_{wet,in} + \frac{\left(c_{p,a} + x_{dry,in}\cdot c_{p,v}\right)}{r}\cdot\left(T_{dry,in} - T_{dry,out}\right) \quad (25)$$

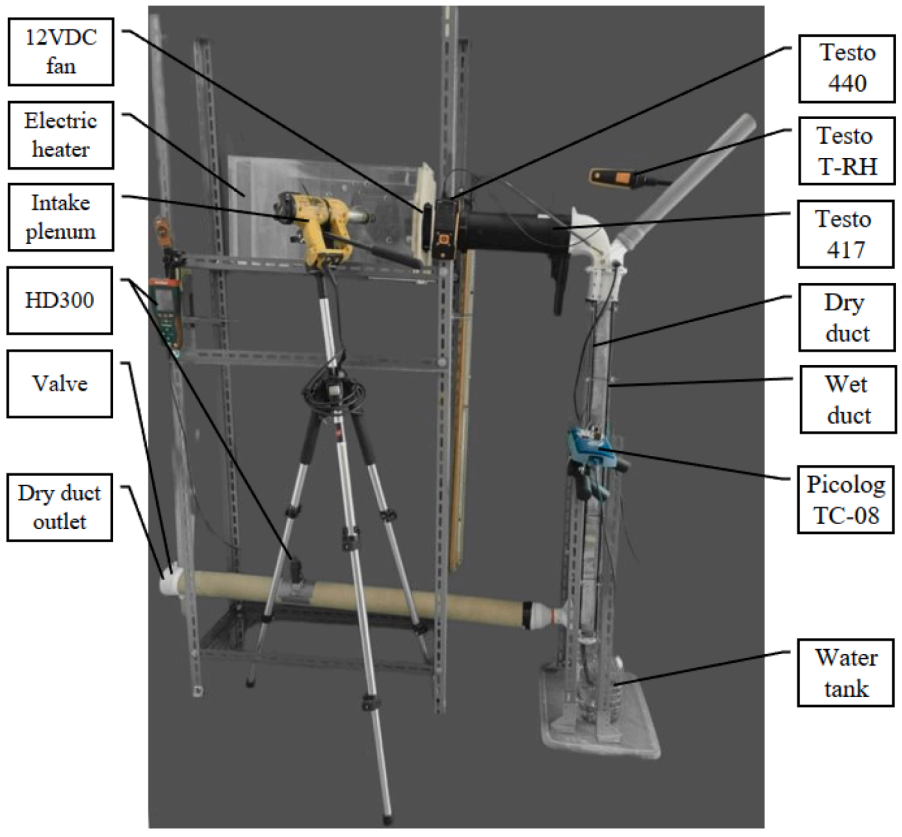

Fig. 7. Experimental setup with the main components and instruments.

The temperature $T_{wet,out}$ (°C) of the air-vapor mixture at the wet channel outlet is then evaluated by the polynomial correlation in Fig. 4. An iterative approach can be used to refine the calculation.

Viscous dissipations take place in both the dry and wet channels. An M-cycle process should be designed to keep such dissipations low. In this regard, the heat rate dissipated due to head loss in the wet and dry channels is as follows:

$$\dot{Q}_{dry} = \dot{V}_{dry} \cdot \Delta p_{dry} \approx \frac{\dot{m}_a \cdot \Delta p_{dry}}{\rho_{a,dry,mean}}$$
$$\dot{Q}_{wet} = r \cdot \dot{V}_{wet} \cdot \Delta p_{wet} \approx \frac{r \cdot \dot{m}_a \cdot \Delta p_{wet}}{\rho_{a,wet,mean}} \quad (26)$$

where Δp_{dry} (Pa) and Δp_{wet} (Pa) are the pressure drops in the two channels due to distributed and concentrated head losses, and the mean volume flow rates are calculated from the dry air density at the mean temperature in the two channels, $\rho_{a,dry,mean}$ and $\rho_{a,wet,mean}$ (kg_a/m^3). In the dry channel, viscous dissipation results in an increment $\Delta T_{dry,out}$ (°C) of the outlet temperature $T_{dry,out}$:

$$\Delta T_{dry,out} = \frac{\dot{Q}_{dry}}{C_{dry}} \quad (27)$$

The increment of $T_{dry,out}$ reverberates in a similar increment $\Delta T_{wet,in}$ (°C) of the wet channel inlet temperature $T_{wet,in}$. In the wet channel, viscous dissipation also results in an increment $\Delta T_{wet,out}$ (°C) of the outlet temperature $T_{wet,out}$ (which is superposed to $\Delta T_{wet,in}$), yet heat is mostly absorbed in terms of latent heat and can be neglected as a first approximation. All this is easily considered in an iterative calculation process.

Significant uncertainties exist on the actual value of *NTU* and, in particular, the value of the overall heat transfer coefficient *UA*. This has been investigated through the test rig described in the following section by measuring the inlet and outlet temperatures of both HMX channels and the mass flow rates with their specific heats. The following flow-chart retraces the main experimental and analytical steps that lead to the validation of the model.

2.2. The experimental setup

To investigate the accuracy of the mathematical model, an experimental setup was created. The design of the setup is based on the dual channel M-cycle design shown in Fig. 2, and a schematic illustration of the experimental apparatus is provided in Fig. 5.

The lab-scale prototype consists of a pre-treatment module of the incoming ambient air that enables the regulation of the air temperature and flow rate. The dry bulb inlet temperature is regulated through an electric heater provided with PID controller, while the air flow is controlled through a 12 VDC variable speed axial fan. The dry and wet duct inlet/outlet temperatures are measured through calibrated T-type thermocouples while relative humidity of the air at the dry duct inlet and wet duct outlet is measured through calibrated Testo 0636–9732 probes connected to a Testo 440 datalogger. The air flow entering the dry duct is measured using a Testo 417 fan anemometer (air flow meter 1 in Fig. 6). At the exit of the dry duct, part of the air is expelled (product air) passing through a second Extech HD300 fan anemometer (air flow meter 2 in Fig. 6) and a butterfly valve which regulates the amount of air recirculated into the wet duct (working air). The working air is humidified through a rack of 3 nozzles which spray distilled water from the top of the HMX. Excess water is collected at the bottom of the wet duct and recirculated through a 12 VDC pump. The water temperature is monitored through the T-type thermocouple. Temperatures measured with thermocouples are recorded using the Picotech TC-08 datalogger.

In Fig. 7 the experimental setup used for model validation is represented, while Table 1 reports the instruments specifications.

The experimental setup allows for four degrees of freedom:

Table 1
List of the instruments used in the experimental campaign.

Instrument	Mesaured variable	Resolution	Uncertainty
Testo 0636-9732	$\varphi_{dry,in}$	1 $\%_{RH}$	± 2$\%_{RH}$
PicoTech TC-08	$T_{dry,in}$, $T_{dry,out}$, T_w, $T_{wet,out}$	0.01 °C	±0.1 °C
Testo 0636-9732	$\varphi_{wet,out}$	0.1 $\%_{RH}$	± 2$\%_{RH}$
Testo 417	$\dot{V}_{dry,in}$	0.01 m s^{-1}	± (0.1 m/s + 1.5 $\%_{m.v.}$)
Extech HD300	$\dot{V}_{dry,out}$	0.01 m s^{-1}	± 3 $\%_{m.v.}$

- the temperature of the air entering the HMX can be varied from ambient temperature to 50 °C by changing the set-point temperature of the electric heater;
- The total air flow rate can be changed by adjusting the 12VCD fan speed up to a maximum of ≈ 40 m^3/h;
- It is possible to adjust the amount of water injected into the wet side of the HMX by varying the duty cycle of the pump.
- The ratio between product and working air can be modified by changing the position of the butterfly valve located downstream of the HD300 flow meter at the dry duct outlet.

The dry and wet duct are separated by a 0.1 mm thick and 1000 mm long aluminum impermeable wall (Fig. 8). The surface has been corrugated so as to maximize the surface area for the same occupied volume, consisting of a series of 10 mm wide partitions for the dry channel alternating with a series of 6 mm wide partitions for the wet channel.

Fig. 9 shows the dimensions of the dry duct and wet duct channels, chosen with different widths according to the different air flow rate flowing in the two channels and in order to have similar air velocity.

Previous tests have shown that smooth aluminum sheet does not allow the homogeneous distribution of water over the entire heat transfer surface.

As observed by Riangvilaikul & Kumal [8] and Xu et al. [10], an homogeneous distribution of water on the heat transfer surface is crucial to allow a more realistic representation of what different mathematical

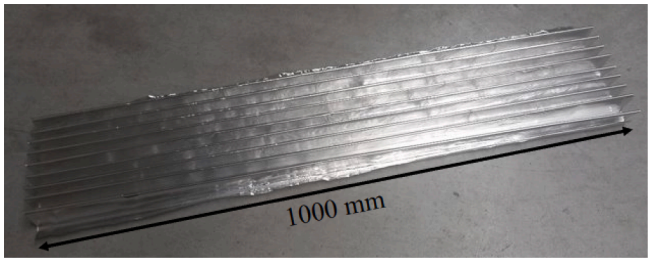

Fig. 8. Original uncoated aluminium sheet heat transfer surface.

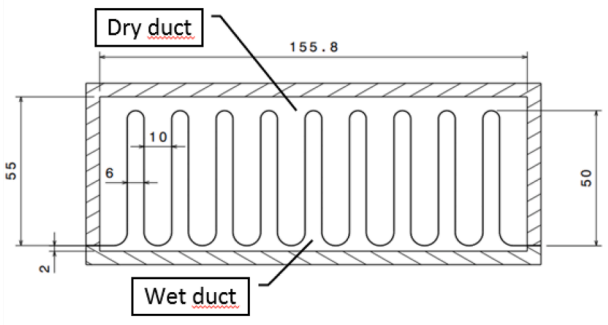

Fig. 9. Dimensions (in mm) of the dry and wet channels.

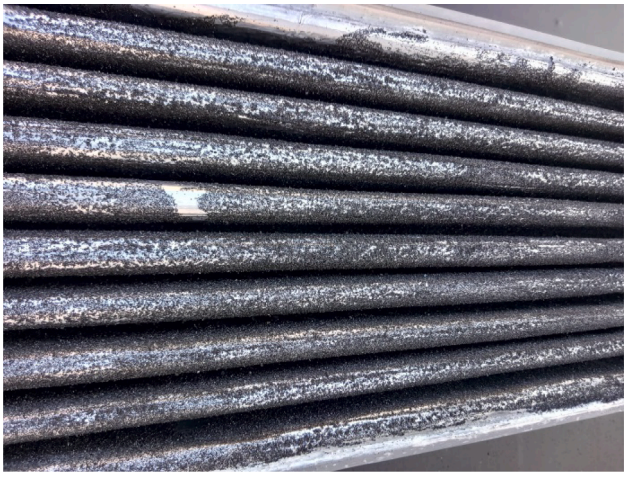

Fig. 10. Char coated heat transfer surface.

models, including the one proposed here, simulate.

It was therefore decided to test a new aluminum heat transfer surface, with an identical geometry to the first one but on which a highly porous vegetable carbon coating was applied on the wet side. The carbonaceous material, well known for its chemical stability and high water retention capacity, was obtained by sieving commercial charcoal according to the ISO 3310-1 reference standard. The grain size of the carbon used for the coating is between 150 and 250 μm. The adhesion of the material to the aluminum surface is guaranteed by a layer of epoxy resin with a total average thickness of the coating of (0.46 ± 0.06) mm. Fig. 10 shows an image of the corrugated heat transfer surface coated with char and Fig. 11 reports a section of the heat transfer surface visualized at the scanning electron microscope (SEM).

2.3. Test method

The experimental tests were conducted by keeping the volumetric flow rate of the air entering the HMX constant at 35 $\frac{m^3}{h}$, while as regards the humidification strategy, it was chosen to spray water at regular intervals: 2 s ON and 60 s OFF. In fact, it was observed that constant spraying induces alterations due to the excessive thermal load absorbed by the liquid water. The water temperature is kept constant during each test at the temperature of 21.0 °C. Before each test, 10 min were waited to ensure that the system operated in steady state regime and, only

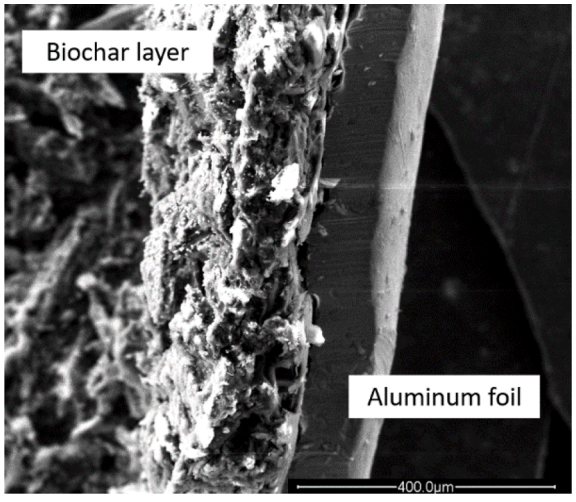

Fig. 11. 300X SEM image of the section of the heat transfer surface coated with char.

Table 2
Experimental results at inlet conditions 22 °C and 29%$_{RH}$.

Test#	$T_{dry,in}$ (°C)	$\varphi_{dry,in}$ (%)	$T_{dry,out}$ (°C)	r (-)	UA (W/K)	NTU (-)	ε (-)
Test 1a	22.08	29.0	16.19	0,401 ± 0.047	14.6 ± 3.99	1.25 ± 0.27	0.57 ± 0.12
Test 2a	22.06	29.0	15.87	0,488 ± 0.043	14.3 ± 3.84	1.23 ± 0.25	0.58 ± 0.12
Test 3a	22.05	29.0	15.35	0,601 ± 0.038	14.9 ± 4.01	1.28 ± 0.26	0.62 ± 0.13
Test 4a	22.05	29.0	15.08	0,715 ± 0.034	15.1 ± 4.19	1.30 ± 0.27	0.64 ± 0.13

subsequently, the temperature, humidity and air flow data were recorded for 5 min through the instruments indicated in Table 1.

The experimental campaign involved the variation of two operating parameters of the HMX:

- Inlet air temperature: tests were conducted both at room temperature (22 °C and 29%$_{RH}$) and by preheating the inlet airflow by means of the electric heater (40 °C and 10%$_{RH}$).
- Recirculation rate: all tests were repeated at 4 different recirculation rates. Each recirculation rate is determined by the position of the butterfly valve located at the dry duct outlet.

The data collected in each test were used as input data of the mathematical model in order to have an estimation of the *UA* value and then to calculate the effectiveness (ε) and *NTU* of the HMX.

2.4. Uncertainty analysis

Uncertainty analysis was carried out to estimate the expected accuracy of the experimental data measurement. The approach employed, as proposed by Klein and McClintock [28] and successfully applied to IEC by Chu et al., 2021 [29], outlines the evaluation of uncertainty in a single-sample experiment using the second-power equation outlined in equation (28).

$$\omega_R = \left[\left(\frac{\partial R}{\partial x_1}w_1\right)^2 + \left(\frac{\partial R}{\partial x_2}w_2\right)^2 + \cdots + \left(\frac{\partial R}{\partial x_n}w_n\right)^2\right]^{\frac{1}{2}} \quad (28)$$

where: R is the result under uncertainty investigation and it is a function of n independent variables x_i (as reported in Eq. (29)) while, ω_i is the known uncertainty correlated to the independent variable x_i and ω_R is the result uncertainty interval.

$$R = f(x_1, x_2, \cdots, x_n) \quad (29)$$

The known uncertainty intervals (ω_i) correlated to a direct measurement (e.g. air temperature, air flowrate, relative humidity etc.) were taken from the instrumentation data sheet and reported in Table 1.

3. Results and discussion

3.1. Experimental results

The experimental campaign was conducted both at the average ambient conditions of temperature and humidity equal to 22 °C and 29 %$_{RH}$, and average preheated conditions of 40 °C and 10 %$_{RH}$.

In each set of inlet temperatures, the air flow rate in the dry channel was kept constant at 35 m^3/h and the product air flow rate was regulated from 8.8 to 21.3 m^3/h, determining 4 different conditions of recirculation rate (r). The variation of the recirculation rate generates a necessary variation of the viscous dissipation of the system which were compensated by regulating the rotation speed of the DC fan.

Table 2 and Table 3 summarize the measured data from the experimental campaign and the calculated parameters used as input in the

Table 3
Experimental results at inlet conditions 40 °C and 10%$_{RH}$.

Test#	$T_{dry,in}$ (°C)	$\varphi_{dry,in}$ (%)	$T_{dry,out}$ (°C)	r (–)	UA (W/K)	NTU (–)	ε (–)
Test 1b	40.00	9.9	21.26	0.731 ± 0.034	16.6 ± 4.74	1.51 ± 0.32	0.70 ± 0.15
Test 2b	39.78	10.0	22.18	0.605 ± 0.038	16.3 ± 4.93	1.48 ± 0.33	0.69 ± 0.15
Test 3b	39.77	10.0	23.52	0.435 ± 0.045	15.6 ± 5.07	1.42 ± 0.34	0.65 ± 0.15
Test 4b	39.74	10.4	24.47	0.360 ± 0.049	15.4 ± 5.31	1.40 ± 0.35	0.63 ± 0.16

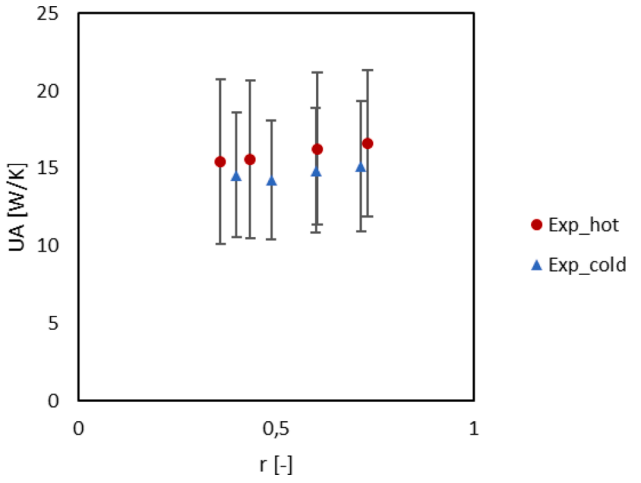

Fig. 12. Calculated values of the overall heat transfer coefficient (UA) vs. recirculation rate (r) with the respective uncertainties.

analytical model.

Uncertainty values are reported along with the calculated data.

The analysis of uncertainty is not often reported in comparisons between numerical models and experimental data, yet error propagation may lead to significant measurement uncertainties. The calculations presented reveal average uncertainties of 29.2% in the calculation of *UA* and 21.7% in the calculation of *NTU*. The calculated uncertainties primarily result from the combination of uncertainties in the measurement of total air flow rate and product air flow rate, which on average are equal to 6% and 3% of their respective measured values. Performing a sensitivity analysis on the error calculation shows that a zeroing of the

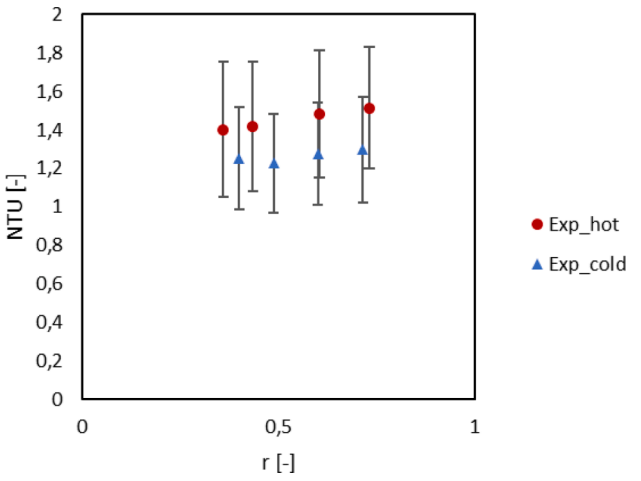

Fig. 13. Calculated values of the NTU vs. recirculation rate (r) with the respective uncertainties.

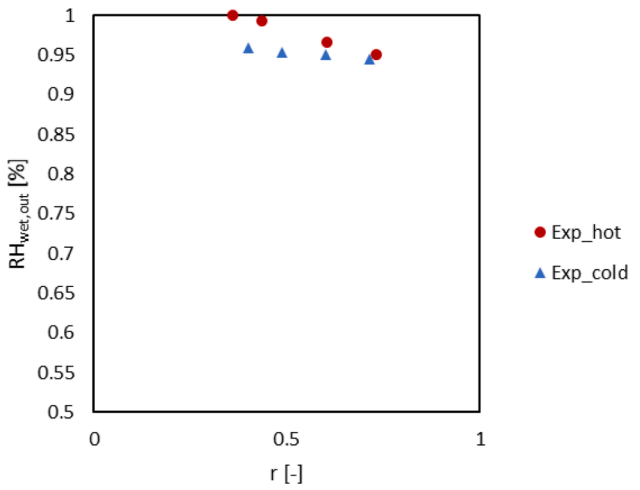

Fig. 14. Variation of relative humidity values exiting the wet channel with changing recirculation rate.

air flow measurement error would result in a halving of the error in the calculated values. Nevertheless, the long measurement chain would not allow an error in measurement of less than 10%.

The uncertainties in temperature and relative humidity measurements are less relevant.

Experimental tests conducted in two very different climatic conditions show how the *UA* trend remains almost constant for both cases and for each investigated recirculation rate. The average value of *UA* is 16.1 W/K in the case of preheated inlet air at 40 °C and 14.8 W/K in the case of tests conducted at room temperature. The measurement uncertainty does not allow effective distinctions of the *UA* value in the two cases; therefore, the numerical model was calibrated using the average value of *UA* for both the sets of tests and equal to 14.9 W/K.

The uncertainties in the calculation of *NTU* are also high and only allow an average estimate of its value, which is equal to 1.5 and 1.3 respectively for the cases of high and low temperature of the inlet air flowrate.

Plots of Figs. 12 and 13 resumes *UA* and *NTU* data collected in Table 2 and 3.

It should be noted that by applying the ε-NTU model as proposed by Liu et al. [20] and calculating the value of *UA* using relationships for the Nusselt number per circular channel through the equivalent diameter, average *UA* values of 3.15 W/K (for 22 °C and 29%$_{RH}$ air inlet

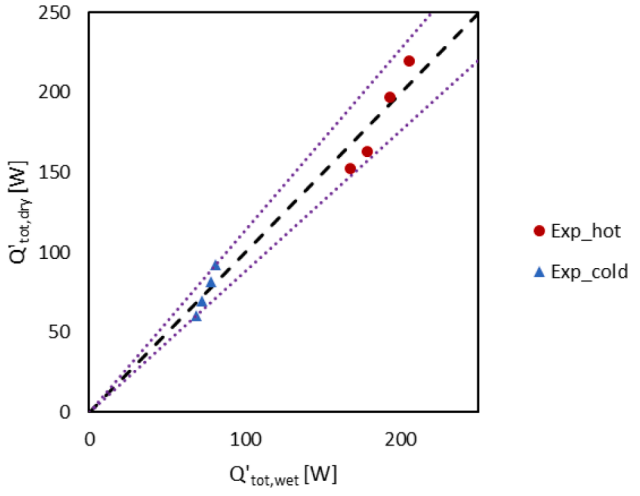

Fig. 15. Energy balance between wet and dry duct. The dotted lines represent the minimum and maximum deviations from the central value.

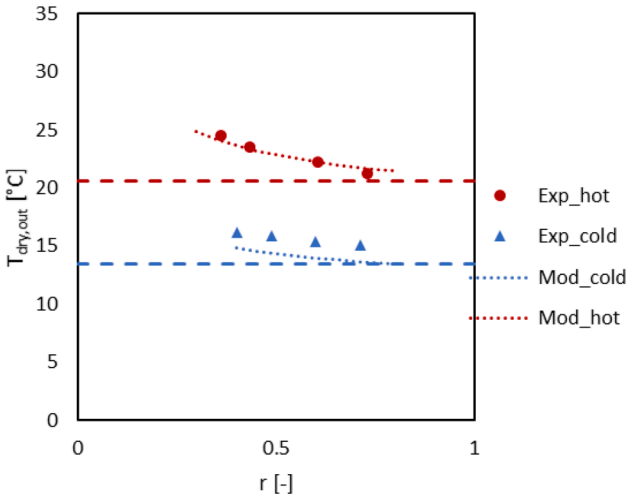

Fig. 16. Dry bulb temperature of the air at the dry duct outlet. Horizontal dashed lines represent the respective wet bulb temperatures of the two different test conditions.

conditions) and 3.24 W/K (for 40 °C and 10%$_{RH}$ air inlet conditions) are obtained. These values are five times lower than the experimentally measured data, highlighting the weakness of the hypotheses applied by Liu et al. as stated by the author themselves.

A strong assumption of the analytical model used is that the air flow in the wet duct is constantly saturated. Only in this way is it possible to estimate the equivalent specific heat capacity with good accuracy. The relative humidity measured at the outlet of the wet duct is reported in Fig. 14, which shows a progressive decrease in performance with increasing recirculation rate. However, the $\varphi_{wet,out}$ values remain close to unity in all tests performed and this condition is also achieved thanks to the adiabatic saturator positioned between the dry duct outlet and wet duct inlet. The impossibility to maintain perfect saturation is a source of error in the calculation and an indication that the evaporative surface should be enhanced to fully exploit the capabilities of the HMX.

The further assumption of adiabaticity of the experimental apparatus was verified by comparing the total thermal power exchanged by the dry duct with the power exchanged in the wet duct. The trends recorded are shown in Fig. 15 and the deviation lines corresponding to a maximum positive deviation of 13.7% and a maximum negative deviation of 12.1% are displayed.

These values are in line with other literature data, whose uncertainties range between 5% and 15% [29–31].

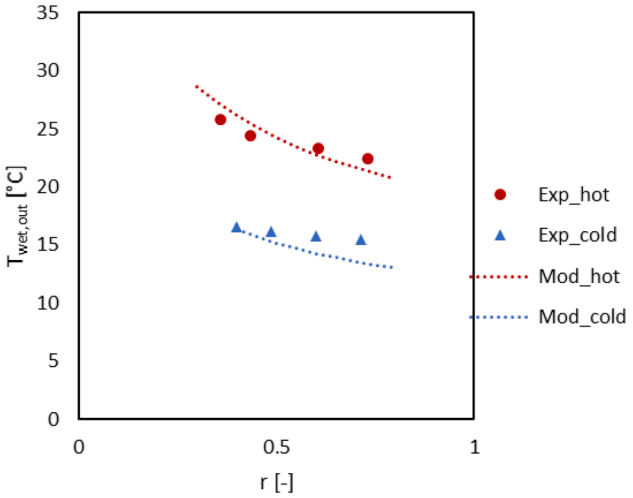

Fig. 17. Dry bulb temperature of the air at the wet duct outlet.

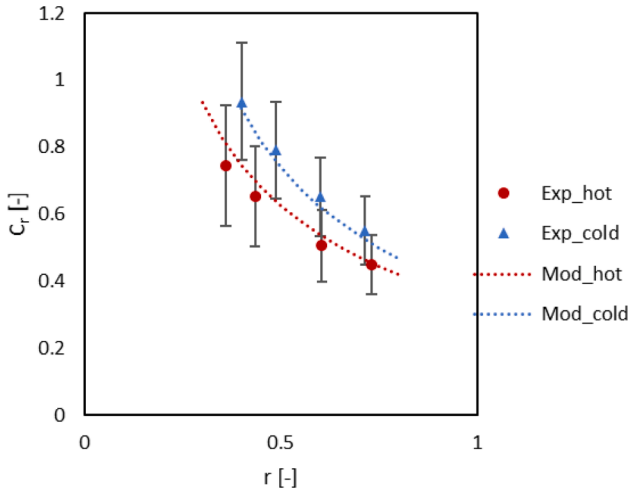

Fig. 18. Trend of the heat capacity ratio function of the recirculation rate (r).

In consideration of the necessary limitations of the experimental apparatus that contains a heat transfer surface with a complex geometry, the following paragraph presents the results generated by the analytical model and compares them with the experimentally obtained data.

3.2. Comparison of experimental and analytical results

The analytical model was validated by inserting the average value of $UA = 14.9$ W/K obtained from the experimental campaign in both climatic conditions.

The results of the analytical model are presented in the series of graphs below. In Figs. 16 and 17, the air temperatures at the outlet of the dry duct and wet duct are shown, respectively. The relative uncertainty of the measured temperature data has not been reported as it is equal to 0.1 °C for each measurement.

In high-temperature tests, the mean difference generated by the model compared to the experimental data is 0.43% for $T_{dry,out}$ while it is 0.11% for $T_{wet,out}$. The discrepancies increase in low-temperature tests, where the errors are 10% and 9.8% respectively compared to the measured value.

For the recorded NTU values (1.5 and 1.3) it is observed that the wet bulb temperature at the dry duct outlet is not reached.

In Figs. 18 and 19, the trend of $C_r = \frac{C_{min}}{C_{max}}$ is compared with the results obtained from the analytical model. Consistent with what was observed for temperatures, the model overestimates the value of C_r in cases with

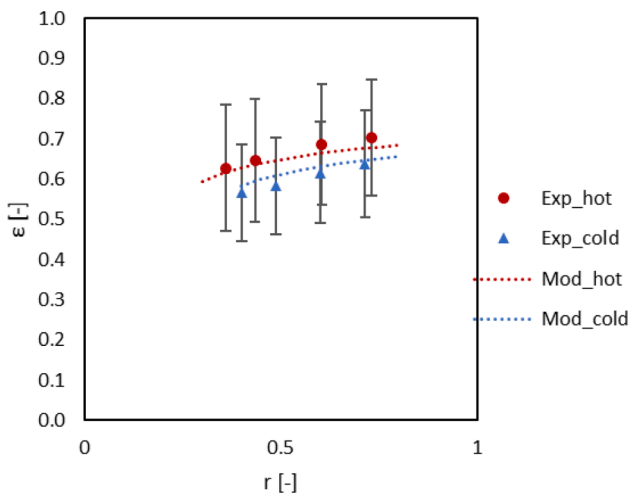

Fig. 19. Trend of the HMX effectiveness in relation to the recirculation rate (r).

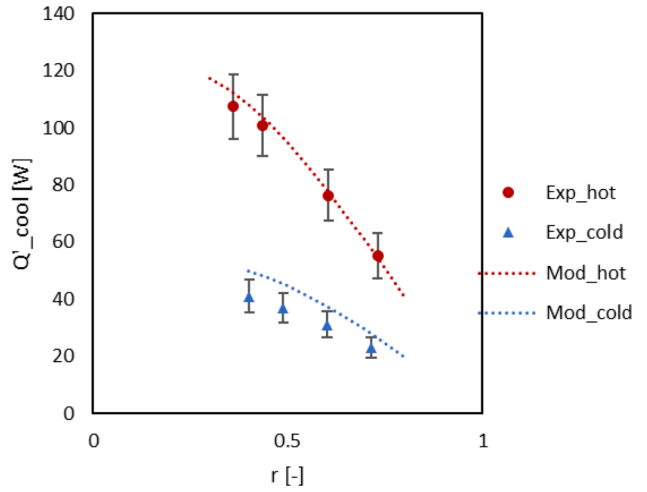

Fig. 20. Useful fraction of the global heat transfer rate referred to the cooling capacity available at the dry duct outlet.

high temperatures and low *RH*. The average deviation from experimental data is 4.8% and 11.2% respectively. Conversely, the trend of efficiency (ε) is underestimated by the model in the case of high inlet temperatures with an average deviation of 2.4%, and 4.3% in the case of room temperature. Measurement uncertainties, in the case of efficiency, rise above 20% as it is at the end of the calculation chain.

On one hand, the temperature value $T_{dry,out}$ decreases as the recirculation rate increases, but the extracted thermal power ($\dot{Q}_{cool}$) decreases in a more than linear manner. Fig. 20 shows the experimental and analytical trends of the thermal power extracted from the dry duct: the estimate offered by the analytical model deviates from the average measured data by 1.2% in the high-temperature case and 10.5% in the ambient temperature case. In this case, the average measurement uncertainties calculated for $\dot{Q}_{cool}$ are 11.5% and 14.4% for the high and low-temperature cases, respectively.

Keeping in mind the limitations dictated by the persistent measurement uncertainty and the use of an overall heat transfer coefficient average for all tests, the model can predict the cases with high air inlet temperature (40 °C) and low relative humidity with great approximation. In cases where HMX operates at temperatures close to 20 °C with average relative humidity rates (40%), The accuracy of the model does not seem to exceed a 10% uncertainty compared to the measured experimental data, values that are however within the limits found in other literature works.

Table 4
Input data for the extension of the analytical calculations.

Parameter	*Value*	*Unit of measurement*
$T_{dry,in}$	35.0	°C
φ_{in}	50.0	%
p_{amb}	101,325	Pa
T_{dp}	23.0	°C
$T_{wb,in}$	26.1	°C
q_{lv} [1]	2500.9	kJ/kg$_l$
$c_{p,eq,mean}$	4324	J/(kg$_a$ K)
Reference fluid properties @ 300 K		
$c_{p,a}$	1006	J/(kg$_a$ K)
R_a	287.05	J/(kg K)
$c_{p,v}$	1864	J/(kg$_v$ K)
c_w	4181	J/(kg$_l$ K)

[1] The latent heat of vaporization has been considered at a temperature of 0 °C.

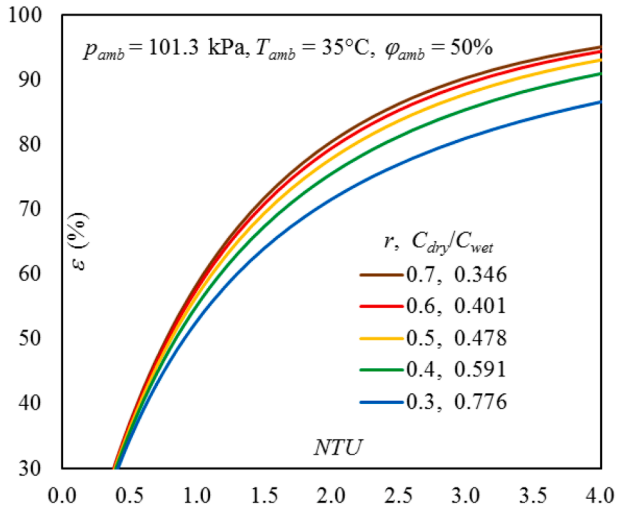

Fig. 21. Heat exchanger effectiveness ε versus *NTU* and fraction *r* of cooled dry air diverted into the wet channel.

3.3. Theoretical performance of the M-cycle and extension of the analytical results

The analytical model, validated through the experimental tests, has therefore been used to investigate the impact of the different operational parameters in more extensive operating conditions than it was possible to obtain experimentally. The input parameters applied to the model are shown in Table 4.

First, the analysis has focused on the mass fraction *r* of cooled air exiting the dry channel, which is diverted to the wet channel and then saturated. Specifically, the impact of r on the effectiveness ε of the heat transfer process has been analyzed since it directly affects the result through the thermal capacity of the air flowing through the wet duct (see Eq. (21)). Naturally, the lower the value of *r*, the higher the fraction (1 - *r*) of cooled air supplied to the air-conditioned environment, and the lower the consumption of vaporized liquid water. A value of *r* between 0.4 and 0.5 appears to be a proper trade-off, allowing a significant increase in ε compared to lower values (see Fig. 21).

Increasing further *r* brings a comparatively small improvement on ε. On the other hand, a high value of *NTU* is needed to achieve a satisfactory value of ε, but this is not simple as the overall heat transfer coefficient *U* through the wall separating the dry and wet channels is negatively affected by the relatively low value of the convection coefficient on the dry side surface. This can be increased by increasing the air velocity and/or promoting turbulence, however viscous losses also increase and, with them, the dissipated energy, which is turned into heat and negatively affects the outlet temperature of the dry channel. Viscous losses also have an impact on the COP of the cooling system as the fan energy absorption increases. Instead, the convection coefficient on the wet side surface can be made relatively high by direct vaporization of liquid water, which is favored by a proper treatment of the wetted surface aimed at promoting retention and spreading of sprayed water. Alternatively, to attain a suitably high *NTU* value, the total heat transfer area A can be increased by elongating the channels or enhancing the cross-sectional perimeter of the channels by introducing corrugations to the partition wall or by applying fins to it. Both actions, however, have a negative impact on viscous losses.

The minimum temperature at which the cooled air is released in standard, direct or indirect, evaporative cooling systems is the wet-bulb temperature $T_{wb,in}$. The M-cycle allows lowering the air temperature $T_{dry,}$

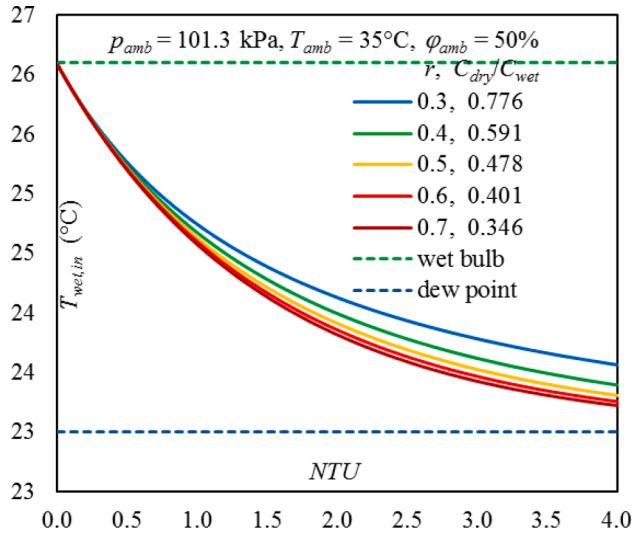

Fig. 22. Cooled air temperature before ($T_{dry,out}$) initial saturation versus *NTU* and fraction *r* of cooled dry air diverted into the wet channel.

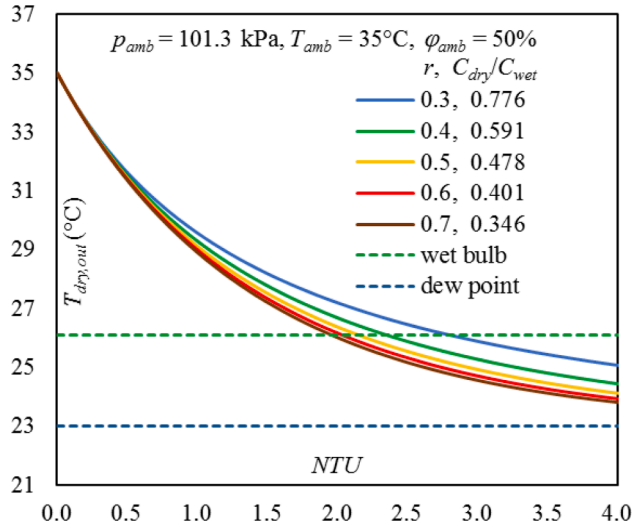

Fig. 23. Cooled air temperature after ($T_{wet,in}$) initial saturation versus *NTU* and fraction *r* of cooled dry air diverted into the wet channel.

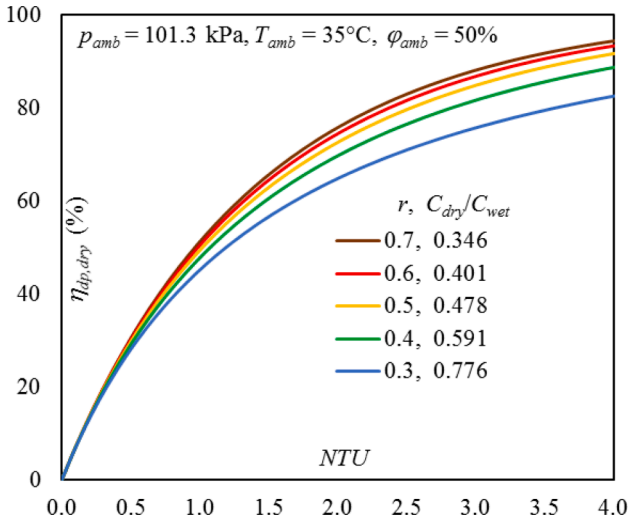

Fig. 24. Dew point efficiency $\eta_{dp,dry}$ (cooled air released at $T_{dry,out}$) versus *NTU* and fraction *r* of cooled dry air diverted into the wet channel.

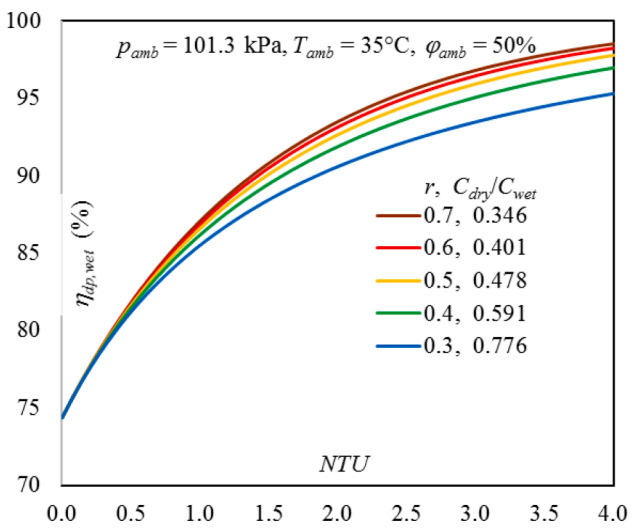

Fig. 25. Dew point efficiency $\eta_{dp,dry}$ (cooled air released at $T_{wet,in}$) versus NTU and fraction r of cooled dry air diverted into the wet channel.

$_{out}$ at the outlet of the dry channel below $T_{wb,in}$, however a relative high effectiveness ε of the heat exchange process is needed. In the reference ambient conditions, a value of ε higher than 80% is required, whichever is the fraction *r* of cooled air that is diverted in the dry channel. On the other hand, saturating the cooled air before releasing it to the cooled environment allows lowering its temperature $T_{wet,in}$ well below $T_{wb,in}$, however at the expenses of a higher consumption of water and a high absolute humidity. A far high NTU value is needed to approach the dew point temperature T_{db} (Fig. 22 and Fig. 23) and *NTU* values higher than 2–2.5 seem necessary to obtain $T_{dry,out}$ lower than the wet bulb temperature, in fact, as shown by the experimental results, NTU values close to 1.5 are not sufficient for this scope.

Translating these considerations to the dew point ($\eta_{dp,dry}$) and wet bulb ($\eta_{dp,wet}$) efficiencies, we construct the graphs in Figs. 24 and 25, where it is once again observed that recirculation rates higher than 0.4–0.5 do not lead to significant improvements in the efficiencies.

4. Conclusions

In this work an analytical method for the study of counter-flow heat exchangers operating according to the Maisotsenko cycle has been studied and validated through a lab-scale HMX prototype. The developed method aims to increase the accuracy of the few analytical approaches available in literature by feeding the ε -NTU method with experimentally measured overall heat transfer coefficient.

In fact, it has been shown that analytical calculation of surface heat transfer fails to correctly predict complex heat transfer geometries or evaporative conditions generated by cold and dry flows.

The proposed modeling approach provides good results in predicting the air outlet temperature from the dry duct and the cooling capacity generated by the lab-scale M-cycle prototype in a wide range of air inlet temperatures.

Extending the model's application beyond what can be verified through the experimental setup, it is observed that the HMX

effectiveness does not increase significantly for r values above 0.4–0.5. The achievement of the wet bulb temperature appears to occur for NTU values around 2–2.5, while achieving the dew point temperature seems to require very high NTU values, prompting research into innovative materials that can ensure a homogeneous water distribution and efficient use.

Declaration of Competing Interest

The authors declare that they have no known competing financial interests or personal relationships that could have appeared to influence the work reported in this paper.

Data availability

Data will be made available on request.

Acknowledgements

Project funded under the National Recovery and Resilience Plan (NRRP), Mission 04 Component 2 Investment 1.5 – NextGenerationEU, Call for tender n. 3277 dated 30/12/2021, Award Number: 0001052 dated 23/06/2022.

References

[1] IEA, Space Cooling, IEA, Paris, 2022. https://www.iea.org/reports/space-cooling, License: CC BY 4.0.
[2] European Commission, A European Green Deal. [online] European Commission, 2020. Available at: https://ec.europa.eu/info/strategy/priorities-2019-2024/european-green-deal_en#actions [Accessed 22 December 2022].
[3] D. Pandelidis, S. Anisimov, Numerical analysis of the heat and mass transfer processes in selected M-Cycle heat exchangers for the dew point evaporative cooling, Energ. Conver. Manage. 90 (2015) 62–83, https://doi.org/10.1016/j.enconman.2014.11.008.
[4] L. Gibbons, S. Javed, A review of HVAC solution-sets and energy performace of nearly zero-energy multi-story apartment buildings in Nordic climates by statistical analysis of environmental performance certificates and literature review, in: Energy, Vol. 238, Elsevier Ltd., 2022, https://doi.org/10.1016/j.energy.2024.121709.
[5] H. Sadighi Dizaji, E.J. Hu, L. Chen, S. Pourhedayat, Development and validation of an analytical model for perforated (multi-stage) regenerative M-cycle air cooler, Appl. Energy 228 (2018) 2176–2194, https://doi.org/10.1016/j.apenergy.2018.07.018.
[6] C. Zhan, X. Zhao, S. Smith, S.B. Riffat, Numerical study of a M-cycle cross-flow heat exchanger for indirect evaporative cooling, Build. Environ. 46 (3) (2011) 657–668, https://doi.org/10.1016/j.buildenv.2010.09.011.
[7] J. il Bang, J.Y. Park, Y.L. Jo, J.W. Jeong, A. Choi, M. Sung, Sterilization effectiveness of in-duct ultraviolet germicidal irradiation system in liquid desiccant and indirect/direct evaporative cooling-assisted 100% outdoor air system, Build. Environ. 186 (2020). https://doi.org/10.1016/j.buildenv.2020.107350.
[8] M. Sung, S. Kato, M. Kim, Development of a fungal biosensor for field verifying the surface disinfection of ultraviolet germicidal irradiation systems for air handling units, Indoor Built Environ. 21 (2) (2012) 273–281, https://doi.org/10.1177/1420326X11409463.
[9] B. Riangvilaikul, S. Kumar, An experimental study of a novel dew point evaporative cooling system, Energ. Build. 42 (5) (2010) 637–644, https://doi.org/10.1016/j.enbuild.16.10.034.
[10] M.H. Mahmood, M. Sultan, T. Miyazaki, S. Koyama, V.S. Maisotsenko, Overview of the Maisotsenko cycle – A way towards dew point evaporative cooling, in: Renewable and Sustainable Energy Reviews, Vol. 66, Elsevier Ltd., 2016, pp. 537–555 https://doi.org/10.1016/j.rser.2016.08.022.
[11] P. Xu, X. Ma, X. Zhao, K. Fancey, Experimental investigation of a super performance dew point air cooler, Appl. Energy 203 (2017) 761–777, https://doi.org/10.1016/j.apenergy.2017.06.095.
[12] Z. Duan, C. Zhan, X. Zhao, X. Dong, Experimental study of a counter-flow regenerative evaporative cooler, Build. Environ. 104 (2016) 47–58, https://doi.org/10.1016/j.buildenv.2016.04.029.
[13] O. Khalid, M. Ali, N.A. Sheikh, H.M. Ali, M. Shehryar, Experimental analysis of an improved Maisotsenko cycle design under low velocity conditions, Appl. Therm. Eng. 95 (2016) 288–295, https://doi.org/10.1016/j.applthermaleng.2015.11.030.
[14] B. Riangvilaikul, S. Kumar, Numerical study of a novel dew point evaporative cooling system, Energ. Build. 42 (11) (2010) 2241–2250, https://doi.org/10.1016/j.enbuild.2010.07.020.
[15] X. Cui, K.J. Chua, W.M. Yang, K.C. Ng, K. Thu, V.T. Nguyen, Studying the performance of an improved dew-point evaporative design for cooling application, Appl. Therm. Eng. 63 (2) (2014) 624–633, https://doi.org/10.1016/j.applthermaleng.2013.11.070.
[16] S.S. Baakeem, J. Orfi, A. Mohamad, S. Bawazeer, The possibility of using a novel dew point air cooling system (M-Cycle) for A/C application in Arab Gulf Countries, Build. Environ. 148 (2019) 185–197, https://doi.org/10.1016/j.buildenv.2018.11.002.
[17] S.S. Baakeem, J. Orfi, A.A. Mohamad, Investigations of geometrical and operational aspects of a dew-point air-cooling system (M-cycle), J. Build. Eng. 36 (2021), https://doi.org/10.1016/j.jobe.2020.102117.
[18] G. Zhu, W. Chen, S. Lu, Modelling of a dew-point effectiveness correlation for Maisotsenko cycle heat and mass exchanger, Chem. Eng. Process. - Process Intesif. 145 (2019), https://doi.org/10.1016/j.cep.2019.107655.
[19] G. Zhu, W. Chen, D. Zhang, T. Wen, Performance evaluation of counter flow dew-point evaporative cooler with a three-dimensional numerical model, Appl. Therm. Eng. 219 (2023), https://doi.org/10.1016/j.applthermaleng.2022.119483.
[20] Z. Liu, W. Allen, M. Modera, Simplified thermal modeling of indirect evaporative heat exchangers, HVAC and R Res. 19 (3) (2013) 257–267, https://doi.org/10.1080/10789669.2013.763653.
[21] S.T. Hsu, Z. Lavan, W.M. Worek, Optimization of wet-surface heat exchangers, Energy 14 (11) (1989) 757–770, https://doi.org/10.1016/0360-5442(89)90009-1.
[22] E. Kozubal, J. Woods, R. Judkoff, Development and Analysis of Desiccant Enhanced Evaporative Air Conditioner Prototype, 2011. http://www.osti.gov/bridge.
[23] J. Woods, E. Kozubal, A desiccant-enhanced evaporative air conditioner: Numerical model and experiments, Energ. Conver. Manage. 65 (2013) 208–220, https://doi.org/10.1016/j.enconman.2012.08.007.
[24] A. Hasan, Going below the wet-bulb temperature by indirect evaporative cooling: Analysis using a modified ε-NTU method, Appl. Energy 89 (1) (2012) 237–245, https://doi.org/10.1016/j.apenergy.2011.07.005.
[25] J. Lehmann, M.C. Rillig, J. Thies, C.A. Masiello, W.C. Hockaday, D. Crowley, Biochar effects on soil biota – A review, Soil Biol. Biochem. 43 (9) (2011) 1812–1836, https://doi.org/10.1016/j.soilbio.2011.04.022.
[26] D. Aller, S. Rathke, D. Laird, R. Cruse, J. Hatfield, Impacts of fresh and aged biochars on plant available water and water use efficiency, Geoderma 307 (2017) 114–121. ISSN 0016-7061. https://doi.org/10.1016/j.geoderma.2017.08.007.
[27] Y.A. Çengel, M.A. Boles, Thermodynamics: An Engineering Approach, 5th ed., McGraw-Hill, 2006.
[28] S.J. Kline, F.A. McClintock, The description of uncertainties in a single sample experiments, Mech. Eng. 75 (1953) 3–8.
[29] J. Chu, W. Xu, Y. Fu, H. Huo, Experimental research on the cooling performance of a new regenerative dew point indirect evaporative cooler, J. Build. Eng. 43 (2021), 102921, https://doi.org/10.1016/j.jobe.2021.102921.
[30] Z. Duan, X. Zhao, C. Zhan, X. Dong, H. Chen, Energy saving potential of a counter-flow regenerative evaporative cooler for various climates of China: Experiment-based evaluation, Energ. Build. 148 (2017) 199–210, https://doi.org/10.1016/j.enbuild.2017.04.012.
[31] S. Anisimov, D. Pandelidis, A. Jedlikowski, V. Polushkin, Investigation of performance of a M (Maisotsenko)-cycle cross-flow heat exchanger for indirect evaporative cooling, Energy 76 (2014) 593–606, https://doi.org/10.1016/j.energy.2014.08.055.